Separation and Purification Technology 319 (2023) 124029

Contents lists available at ScienceDirect

Separation and Purification Technology

journal homepage: www.elsevier.com/locate/seppur

KH570 firmly anchors Ag^{+}/Ag^{0} on TiO_2 nanotubes to enhance organics removal during photocatalytic activation of peroxymonosulfate

Jialin Jia [a,b], Stefanos Giannakis [c], Dong Li [b,d,*], Tao Lin [a], Jiayu Tian [e], Dongmei Liu [b,*], Jun Ma [b]

[a] Key Laboratory of Integrated Regulation and Resource Development on Shallow Lakes of Ministry of Education, College of Environment, Hohai University, Nanjing 210098, China
[b] State Key Laboratory of Urban Water Resource and Environment, School of Environment, Harbin Institute of Technology, Harbin 150090, China
[c] Universidad Politécnica de Madrid, E.T.S. Ingenieros de Caminos, Canales y Puertos, Departamento de Ingeniería Civil: Hidráulica, Energía y Medio Ambiente, Unidad docente Ingeniería Sanitaria, c/ Profesor Aranguren, s/n, ES-28040 Madrid, Spain
[d] Collaborative Innovation Center of Atmospheric Environment and Equipment Technology, Jiangsu Key Laboratory of Atmospheric Environment Monitoring and Pollution Control, School of Environmental Science and Engineering, Nanjing University of Information Science & Technology, Nanjing 210044, China
[e] School of Civil and Transportation Engineering, Hebei University of Technology, Tianjin 300401, China

ARTICLE INFO

Keywords:
Peroxymonosulfate
Photocatalysis
Silver
KH570
Bisphenol A

ABSTRACT

To enhance the photocatalytic activation of peroxymonosulfate (PMS), the precious metal was used to modify the catalyst. However, the catalyst suffered from metal leaching due to the oxidation of zero-valent metal into the ionic state by PMS. Herein, the silane coupling agent, KH570, was selected to fix metal Ag on the surface of TiO_2 nanotubes arrays (TiO_2NTAs) firmly and dispersedly. The prepared Ag/KH570/TiO_2NTAs were efficient visible-light (VL) photocatalytic PMS activators for the degradation of bisphenol A (BPA). The Ag/KH570/TiO_2NTAs/PMS/VL system exhibited a higher degradation rate (k_{obs} = 0.1 min^{-1}) and exceptional stability even after 30 cycles (0.098 min^{-1}) compared to Ag/TiO_2NTAs/PMS/VL system (0.074 and 0.015 min^{-1} for first and fourth use, respectively). KH570 well-dispersed Ag^0 on the surface of TiO_2NTAs showed significantly enhanced VL absorption, photo-generated current, and electro-transfer ability, which boosted PMS activation. The Ag^0 also activated PMS and converted to Ag^+, which was quickly reduced to Ag^0 again by photo-generated electrons. KH570 well-immobilized Ag^0/Ag^+ promoted above catalytic cycles with minimal Ag leaching. Activation of PMS by the photo-generated electrons and Ag^0 resulted in the generation of •OH and $SO_4^{\bullet-}$, which seized the principal position for BPA removal. The wide pH adaptability and production of more oxidant in water matrixes (Cl^-, HCO_3^-, and humic acid) enabled Ag/KH570/TiO_2NTAs/PMS/VL system to exhibit excellent performance in the actual waterbodies (groundwater and tap water). This work would provide useful information in the construction of stable zero-valent metal modified catalysts for the (photo)catalytic activation of PMS/persulfate.

1. Introduction

Advanced oxidation processes based on peroxymonosulfate (PMS) have been extensively regarded as efficient methods for the elimination of organic compounds [1,2]. PMS cannot only oxidize organic pollutants in water itself, but also be activated to form other reactive oxygen species (such as $SO_4^{\bullet-}$, •OH, and $^1O_2$) to oxidize organics [3–5]. Approaches to activate PMS include ultraviolet radiation [6], ultrasound [7], thermolysis [8], homogeneous/heterogeneous catalysis [9,10], etc. Among them, heterogeneous catalytic activation has received widespread attention due to the cost-effectiveness, strong applicability, and sustainability of catalyst [1]. Metal oxides are one of the most commonly used catalysts. The activation process usually follows the redox reaction of the variable valence metals with PMS to form reactive species [11]. Some metal oxide semiconductors (TiO_2, BiOCl, Fe_2O_3, Bi_2MoO_6, etc) can conduct photocatalytic activation of PMS via the photo-generated electrons to convert PMS into reactive oxidants [12–16]. This process combines the dual merits of photocatalysis and PMS activation oxidation. Besides, the element doped metal oxide, single atom modified metal oxide, and composite metal oxide are developed to improve the performance of photocatalytic activation of PMS [17–25]. Nevertheless, the activity of these catalysts decreases apparently after several cycles of operation, and/or the powder catalysts are difficult to separate and recycle, which is easy to cause secondary pollution.

* Corresponding authors.
E-mail addresses: lidong890210@126.com (D. Li), ldm819@126.com (D. Liu).

https://doi.org/10.1016/j.seppur.2023.124029
Received 10 March 2023; Received in revised form 29 April 2023; Accepted 4 May 2023
Available online 8 May 2023
1383-5866/© 2023 Elsevier B.V. All rights reserved.

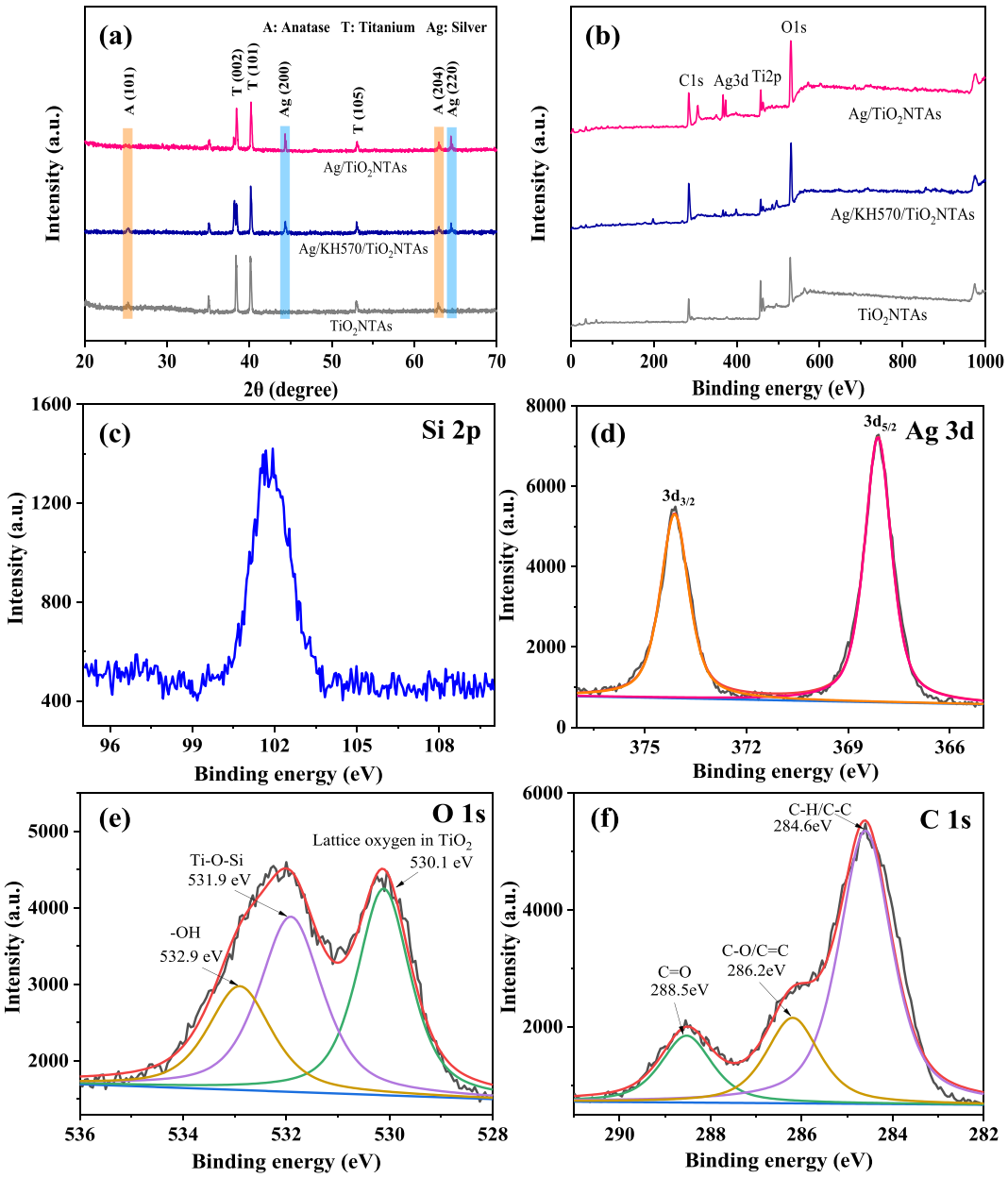

Fig. 1. XRD patterns of catalysts (a); Full-scale XPS spectra of catalysts (b); High-resolution spectra for Si 2p (c), Ag 3d (d), O 1s (e), and C 1s (f) of Ag/KH570/TiO_2NTAs samples.

Among metal oxides, TiO_2 nanomaterials have been widely studied in the field of photocatalytic water purification due to their advantages of chemical stability, cheapness, and non-toxicity [26–28]. To improve the practicability of TiO_2, TiO_2 nanotubes arrays (TiO_2NTAs) were synthesized vertically on Ti-metal substrate by electrochemical anodization [15,29]. The oriented tubular structure of TiO_2NTAs provides exceptional charge transport and light harvesting capabilities [30]. Moreover, the chemical bonding of TiO_2NTAs to the Ti-substrate enables easy recovery of the catalyst for long-term usage. Nevertheless, the low VL absorption of TiO_2NTAs hinders its application. To solve this disadvantage, TiO_2NTAs are modified with noble metals [29,31,32]. For instance, surface plasmon resonance (SPR) of zero-valent silver (Ag^0) can enhance the utilization of VL [33]. Usually, Ag^0 is loaded onto the TiO_2NTAs surface without chemical bonding through the deposition method [34,35]. To our knowledge, the Ag^0-modified TiO_2 photocatalyst for PMS activation has been rarely reported. The reason may be that the addition of PMS oxidizes Ag^0 into ionic state and reduces its load stability. Previous studies have reported that silane coupling agents can improve the adhesion of catalyst through their powerful "bridging" effect [36–38]. Their molecular structure can be expressed as Y-R-SiX3. The -X represents halogen, acetoxy, alkoxy, etc., and their hydrolysis can result in the generation of silanol hydroxyl groups (-Si-OH), which can bond to the surface of inorganic materials through hydrogen bonding or dehydration [38]. The -Y represents amino, mercapto, vinyl (alkene), etc, which can chelate/coordinate metals [39–42]. Given the adhesion function of silane coupling agents, they can be used to connect Ag^0 with TiO_2NTAs for improving its stability in PMS activation.

Herein, the silane coupling agent, KH570, was attempted to immobilize metal Ag on the surface of TiO_2NTAs. The prepared Ag/KH570/TiO_2NTAs were applied for photocatalytic activation of PMS by VL (Ag/KH570/TiO_2NTAs/PMS/VL) to degrade bisphenol A (BPA), a typical endocrine disruptor that is frequently detected in various water environment and can produce toxic effects after entering the human body [43]. KH570 fixed Ag nanoparticles enhanced BPA removal and

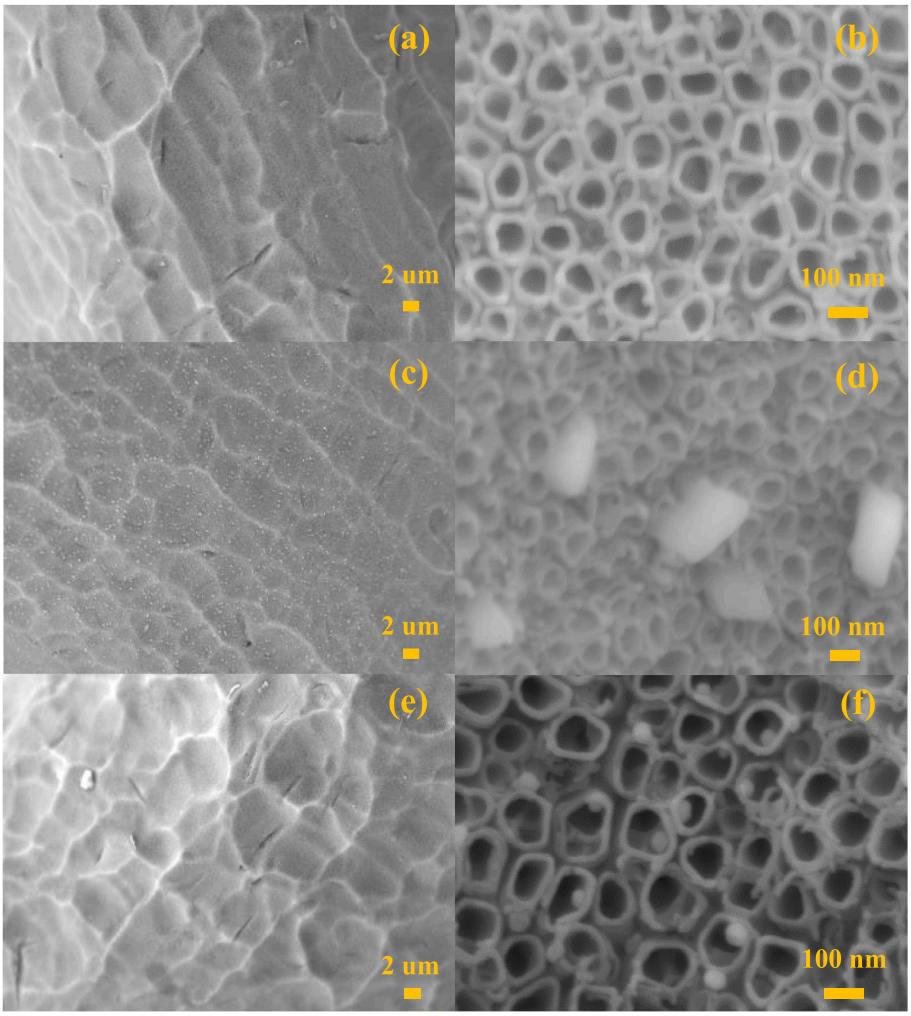

Fig. 2. SEM images of TiO_2NTAs (a, b), Ag/TiO_2NTAs (c, d), and Ag/KH570/TiO_2NTAs (e, f).

achieved long-term stable PMS activation. The reactive species for oxidation of BPA were identified, and the probable reaction mechanism was proposed. Additionally, the effects of reaction parameters and water matrixes on the degradation performance were investigated. Finally, BPA removal in real waterbodies by Ag/KH570/TiO_2NTAs/PMS/VL system was evaluated.

2. Materials and methods

2.1. Chemicals and reagents

Chemicals and reagents were provided in Supplementary Materials (Text S1).

2.2. Preparation of Ag/KH570/TiO_2NTAs

The preparation process of Ag/KH570/TiO_2NTAs was illustrated in Fig. S1. First, TiO_2NTAs were prepared on Ti mesh using the anodization method. The detailed procedures are described in Text S2. Second, TiO_2NTAs were immersed into 50 mL mixed solution (water: ethanol = 1:1 in volume) containing 0.25 g KH570, and the solution was continuously stirred for 60 min at 80 °C to obtain KH570 coated TiO_2NTAs (KH570/TiO_2NTAs). Afterward, KH570/TiO_2NTAs were washed with ethanol to remove the residual KH570, and dried at 60 °C for 120 min. Third, Ag-decorated KH570/TiO_2NTAs (Ag/KH570/TiO_2NTAs) were synthesized by photodeposition, which was irradiated by 300 W Xenon lamp in 0.01 mol/L $AgNO_3$ solution for 60 min. The obtained Ag/KH570/TiO_2NTAs were rinsed with deionized water and dried at 60 °C for 1 h. For comparison, Ag directly deposited TiO_2NTAs without KH570 pretreatment were also prepared and named Ag/TiO_2NTAs. The methods of characterization of catalyst were given in Text S3.

2.3. Evaluation of degradation performance

The schematic diagram of the experimental device was depicted in Fig. S2. BPA degradation experiments were performed in a 100 mL beaker containing 50 mL BPA (10 mg/L). The VL was provided using a 300 W Xenon lamp equipped with a 400 nm cut-off filter. The light intensity on the catalyst surface was 70 mW/cm^2. The reaction area of catalyst was 1 × 2 cm^2. The reaction solution was sampled at specified time intervals, filtered with 0.22 μm PTFE membrane and injected into a vial containing excessive methanol (MeOH) to terminate the reaction. The BPA concentration was determined by an ultra-performance liquid chromatography (UPLC, Waters, USA) equipped with a BEH C18 column (1.0 mm × 50 mm × 1.7 μm) and a UV detector (λ = 230 nm). The mobile phase was comprised of methanol and ultrapure water (V/V = 65/35) at a flow rate of 0.1 mL/min. The concentration of Ag ion in solution was determined with an inductively coupled plasma mass spectrometry (ICP-MS, NexION300Q, PerkinElmer). The PMS concentration was quantified with the ABTS method on a UV–Vis spectrophotometer (T6, PERSEE).

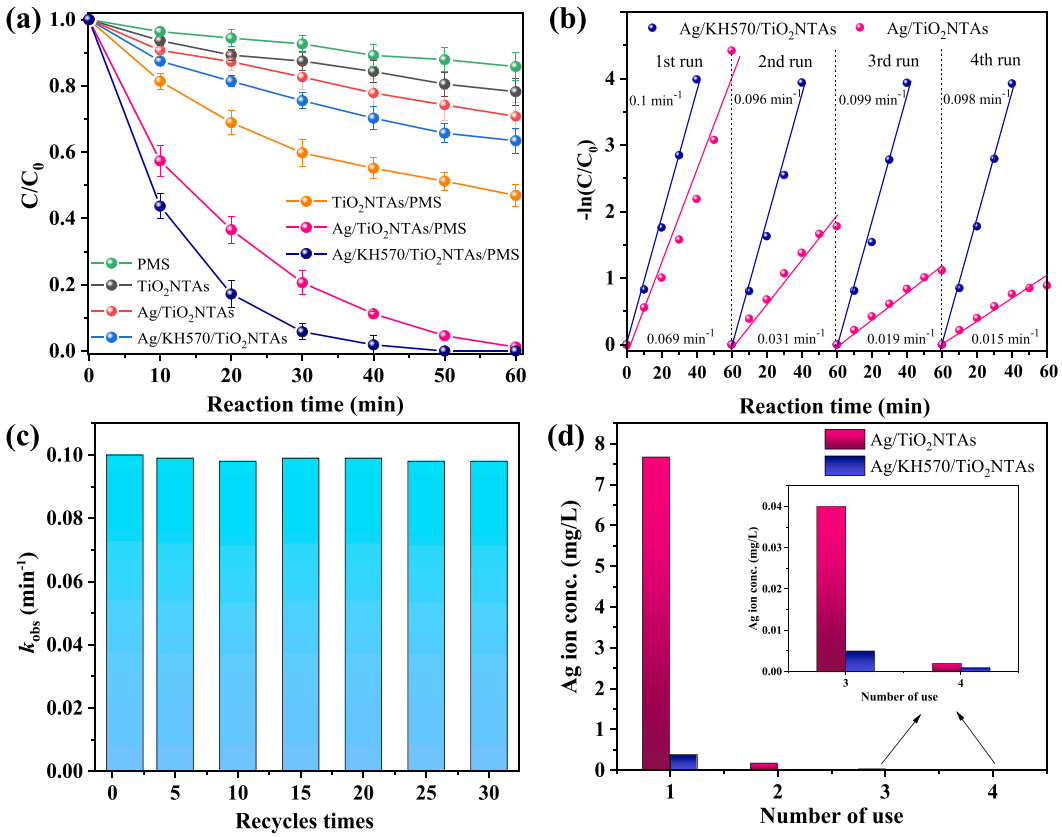

Fig. 3. (a) BPA removal efficiency in different reaction systems under visible light; (b) Kinetics of BPA removal for consecutive four cycles in Ag/KH570/TiO_2NTAs/PMS/VL and Ag/TiO_2NTAs/PMS/VL systems; (c) Long-term BPA removal in Ag/KH570/TiO_2NTAs/PMS/VL system; (d) Ag leaching concentration in (b). Experimental conditions: $[PMS]_0$ = 0.5 mM, $[BPA]_0$ = 10 mg/L, $[pH]_0$ = 4.0, T = 25°C.

2.4. Photoelectrochemical measurement

The photoelectrochemical properties of the samples were analyzed on a CHI760E electrochemical workstation. In a typical three-electrode system, the Pt electrode, saturated calomel electrode (SCE), and prepared catalyst were used as the counter electrode, reference electrode, and work electrode, respectively. The 0.5 M of Na_2SO_4 solution and a 300 W Xenon lamp with a 400 nm cut-off filter were employed as supporting electrolyte and light source, respectively.

3. Results and discussion

3.1. Characterization of Ag/KH570/TiO_2NTAs catalyst

Fig. 1a shows the XRD patterns of the catalysts. All samples exhibited the obvious phase of Ti metal at 38.4°, 40.2°, and 53.1° (JCPDS NO. 44–1294). The diffraction peaks at 25.6° and 63.1° belonged to (101) and (204) crystal planes of anatase TiO_2 (JCPDS NO. 21-1272), respectively [44]. Both Ag/TiO_2NTAs and Ag/KH570/TiO_2NTAs exhibited two Ag^0 peaks at 44.4° and 64.5°, corresponding to the (200) and (220) planes, respectively [33,45]. Notably, the (101) crystal plane of TiO_2 in Ag/TiO_2NTAs disappeared, possibly due to the covering of metal Ag. Compared with Ag/TiO_2NTAs, Ag/KH570/TiO_2NTAs clearly showed lower peak intensity and wider peak width (half height) for diffraction peak of Ag^0. According to the Debye-Scherrer formula, the size of Ag^0 particle in Ag/KH570/TiO_2NTAs samples was smaller than that in Ag/TiO_2NTAs samples. This indicated that Ag^0 particles might aggregate on the surface of TiO_2NTAs, while KH570 could disperse Ag^0 particles.

The elemental composition and chemical state of the catalysts were analyzed by XPS measurement. The C, Ag, O, and Ti elements were observed in Ag/KH570/TiO_2NTAs full-scale spectrum (Fig. 1b), while the Si element could be only found in the high-resolution spectrum due to its weak intensity (Fig. 1c). The peak intensity of Ag element in Ag/TiO_2NTAs exceeded that in Ag/KH570/TiO_2NTAs (Fig. 1b and 7). It suggested that Ag content in Ag/TiO_2NTAs samples was higher under the same photo-reduction time. The high-resolution Ag 3d spectrum of Ag/KH570/TiO_2NTAs exhibited two Ag^0 peaks at 374.1 and 368.1 eV (Fig. 1d) [46]. The O 1 s spectrum was divided into three peaks (Fig. 1e). The peaks at 530.1, 531.9, and 532.9 eV were indexed to the lattice oxygen of TiO_2, Ti-O-Si bond, and adsorbed –OH, respectively [47–49]. The C 1 s spectrum also consisted of three peaks (Fig. 2f). The peak of 284.6 eV was attributed to the C–H or C–C bonds of adventitious carbon. The C=C/C–O (286.2 eV) and C=O (288.5 eV) bonds were ascribed to the introduction of KH570 [50]. Overall, the XPS results indicated that KH570 was successfully grafted onto the surface of TiO_2NTAs, and the Ag element existed in the form of zero-valent Ag, which was consistent with the XRD result.

The morphologies of catalysts were shown in Fig. 2. TiO_2NTAs presented a smooth nanotube surface. In the SEM images of Ag/TiO_2NTAs, the large cubic Ag^0 particles of 200–250 nm were deposited on the surface of TiO_2NTAs. Nevertheless, the introduction of KH570 resulted in the generation of smaller Ag^0 nanoparticles, with a size of around 50 nm. Nanoscale metal particles would provide more active sites, which were more conducive to the catalytic reaction. Previous literature has indicated that KH570 could stabilize nanoparticles and prevent their aggregation via a bridging effect [38]. Hence, the bridging function of KH570 restrained the growth of Ag^0 particles during the photo-reduction deposition of Ag ions.

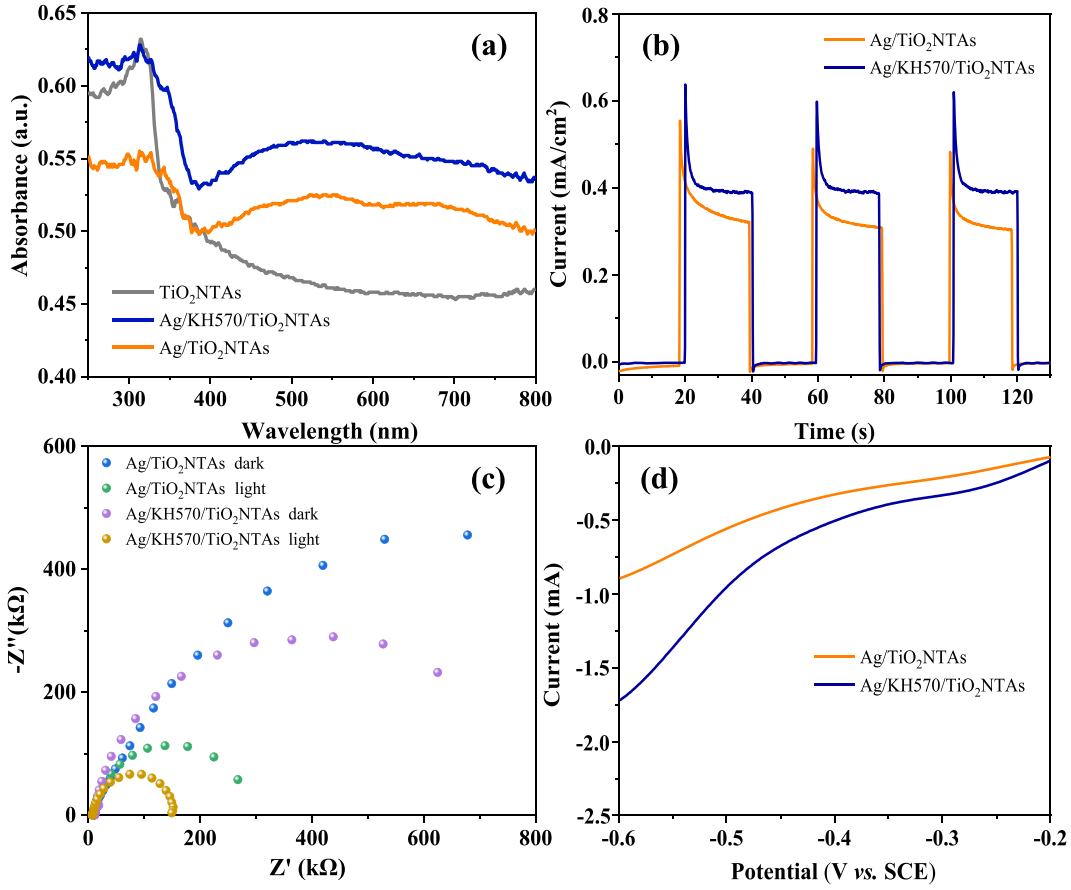

Fig. 4. UV–Vis DRS (a) and photo-electrochemical properties (transient photocurrent response spectra for (b), electrochemical impedance spectroscopy Nyquist plots for (c), and linear sweep voltammetry curves for (d)) of Ag/TiO_2NTAs and Ag/KH570/TiO_2NTAs.

3.2. Evaluation of catalytic performance

The photocatalytic activation of PMS by the prepared catalyst was performed for the degradation of BPA, as shown in Fig. 3. The previous study confirmed that the direct VL photolysis hardly removed BPA [16]. The BPA removals by catalysts adsorption were also ineffective (<10%) (Fig. S3). Even after the addition of PMS, improvement in degradation efficiency was not profound. The BPA degradation rates in PMS/dark, TiO_2NTAs/PMS/dark, Ag/TiO_2NTAs/PMS/dark, and Ag/KH570/TiO_2NTAs/PMS/dark systems were 10.5%, 15.5%, 19.2%, and 20.3%, respectively (Fig. S3). These indicated that the catalysts had a weak ability to activate PMS in dark. The alone photocatalytic processes showed measurable BPA removals (Fig. 3a), which were 14.2%, 21.8%, 29.2%, and 36.6% for PMS/VL, TiO_2NTAs/VL, Ag/TiO_2NTAs/VL, and Ag/KH570/TiO_2NTAs/VL systems, respectively. The deposition of Ag^0 improved BPA removal apparently, while the introduction of KH570 further promoted its degradation. Additionally, when PMS was added, distinct enhancements of BPA degradation in TiO_2NTAs/PMS/VL, Ag/TiO_2NTAs/PMS/VL, and Ag/KH570/TiO_2NTAs/PMS/VL systems were achieved, with removal efficiencies of 53.1%, 98.8%, and >99.9% within 60 min, respectively. The BPA degradation data were well-fitted with the pseudo-first-order kinetic model. The rate constant of Ag/KH570/TiO_2NTAs/PMS/VL system was 0.099 min^{-1}, which was 1.4 and 8.3 times that of Ag/TiO_2NTAs/PMS/VL (0.069 min^{-1}) and TiO_2NTAs/PMS/VL systems (0.012 min^{-1}), respectively (Fig. S4). The Ag content in Ag/KH570/TiO_2NTAs was around 5 wt% (The Ag content of Ag/KH570/TiO_2NTAs in the full text was 5% unless otherwise stated), which was the optimal amount (Fig. S5). The other Ag content (including 1 wt%, 2 wt%, and 10%) modified samples also performed higher performance than TiO_2NTAs, confirming the critical role of Ag for the enhancement of photocatalytic activation of PMS (Fig. 3a and S5). It was worth noting that Ag content in the Ag/TiO_2NTAs exceeded that of Ag/KH570/TiO_2NTAs (Fig. 1b and 6). The results indicated that the addition of KH570 not only reduced the use of metal Ag but also enhanced the removal of BPA.

The stability of the catalyst is the key to ensuring its continuous application. To further highlight the role of KH570, cyclic experiments were conducted. As depicted in Fig. 3b and S6, BPA removal efficiency of Ag/TiO_2NTAs/PMS/VL remarkably decreased as the cycle times increased. After four cycles, BPA degradation efficiency was only 54.9%, which was almost equal to that of the TiO_2NTAs/PMS/VL system (53.1%). In contrast, Ag/KH570/TiO_2NTAs/PMS/VL system could maintain highly efficient and stable BPA removal, even after 30 cycles (Fig. 3c). The decrease in BPA removal efficiency of Ag/TiO_2NTAs/PMS/VL might be due to a large amount of Ag leaching, while KH570 in Ag/KH570/TiO_2NTAs could well anchor Ag on the surface of TiO_2NTAs (Fig. 3d, S7, and 6). KH570 could potentiate the adhesion between Ag and TiO_2NTAs through the "bridging" function, in which the vinyl group in KH570 could coordinate the Ag metal and the silanol hydroxyl groups in KH570 would connect with TiO_2 [38,42]. The Ag leaching content in Ag/KH570/TiO_2NTAs (excepting first use) could meet the requirement (<0.05 mg/L) of Standards for drinking water quality in China (GB 5749–2022). Furthermore, more decomposition of PMS by the used Ag/KH570/TiO_2NTAs further demonstrated its catalytic potential (Fig. S8). Compared with other immobilized catalysts listed in Table S1, Ag/KH570/TiO_2NTAs exhibited superior pollutant removal efficiency and catalytic stability, as well as reduced oxidant dosage. It was worth noting that regardless of whether the Ag content in Ag/TiO_2NTAs was higher or lower than that in Ag/KH570/TiO_2NTAs, the BPA removal efficiency in Ag/TiO_2NTAs/PMS/VL system was consistently lower than

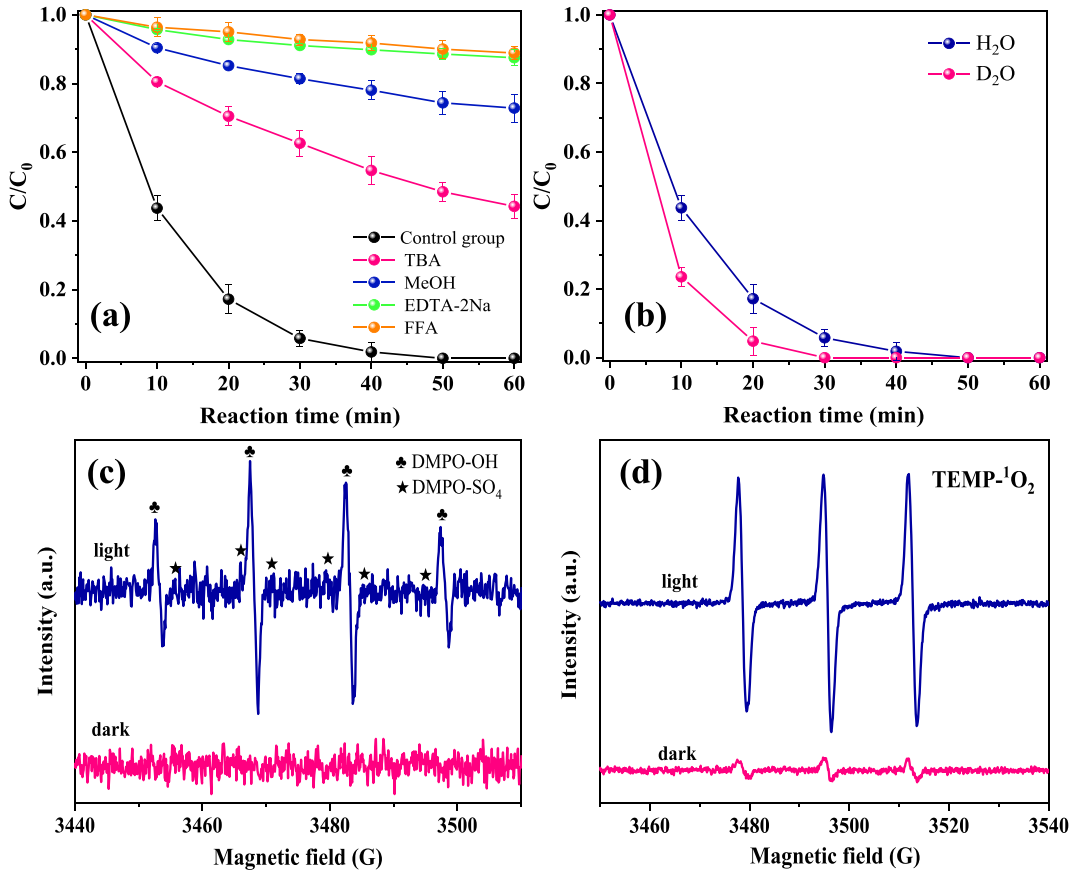

Fig. 5. Effects of various quenchers on BPA degradation (a); BPA degradations in H_2O and D_2O systems (b); DMPO (c) and TEMP (d) spin-trapping EPR spectra. Experimental conditions: Ag/KH570/TiO_2NTAs/PMS/VL system, $[PMS]_0$ = 0.5 mM, $[BPA]_0$ = 10 mg/L, $[TBA]_0$ = $[MeOH]_0$ = $[EDTA\text{-}2Na]_0$ = 10 mM, $[FFA]_0$ = $[TEMP]_0$ = 20 mM, $[DMPO]_0$ = 50 mM, $[pH]_0$ = 4, T = 25℃.

that of Ag/KH570/TiO_2NTAs/PMS/VL system (Fig. 1b, 3, and S7). Therefore, it could be inferred that at the same Ag content, the BPA removal performance of catalysts with KH570 would still surpass that without KH570.

3.3. Catalytic oxidation mechanism

The effect of KH570 on light absorption of Ag/TiO_2NTAs was studied (Fig. 4a). UV–Vis diffuse reflectance spectra (DRS) showed that TiO_2NTAs had ultraviolet light absorption and a small amount of VL absorption due to its band-gap energy of 2.95 eV (Fig. S9). The Ag/TiO_2NTAs and Ag/KH570/TiO_2NTAs exhibited strong absorption in the VL region, which was attributed to the surface plasmon resonance of Ag metal [51]. By comparison, stronger absorptions in Ag/KH570/TiO_2NTAs were observed relative to Ag/TiO_2NTAs in both ultraviolet light and VL regions. The KH570 restrained the growth of Ag^0 particles and made Ag^0 nanoparticles disperse well on the surface of TiO_2NTAs, resulting in the formation of more VL absorption sites to induce surface plasmon resonance. After four cycles, Ag/KH570/TiO_2NTAs still showed high ultraviolet light and VL absorption, while Ag/TiO_2NTAs exhibited a decrease in VL absorption due to Ag leaching, in which the curves was almost overlapped with that of TiO_2NTAs (Fig. S10a).

The photo-generated electrons and electron-transfer performances affect the generation of reactive oxygen species and the degradation of pollutants in the photocatalytic activation of the PMS process. Thus, the photo-electrochemical performances of the catalysts were studied to analyze the mechanism of enhanced pollutant removal. In Fig. 4b, the samples with KH570 elevated photocurrent value apparently, indicating that more light absorption would lead to more photo-generated electrons. Also, the introduction of KH570 maintained a stable photo-generated current (Fig. S10b), which corresponded well with DRS results. Moreover, a smaller arc radius in the electrochemical impedance spectroscopy Nyquist plots (Fig. 4c) and a higher current in the linear sweep voltammetry curves (Fig. 4d) of the Ag/KH570/TiO_2NTAs suggested its low interface electron-transfer resistance and excellent electron-transfer capacity, respectively. The well-dispersed nanoscale Ag^0 particles in Ag/KH570/TiO_2NTAs could maximize the utilization of photo-generated electrons, and the KH570 modification did not influence the transfer of photo-generated electrons (Ag^0 nanoparticles not only connected with KH570 but also directly contacted with TiO_2NTAs). The more photo-generated electrons and fantastic electron-transfer ability could effectively boost PMS activation to produce abundant reactive species for BPA removal.

Scavenging experiments were carried out to identify the reactive species. MeOH and *tert*-butyl alcohol (TBA) were used to distinguish the contribution of $SO_4^{\bullet-}$ and •OH. Although both are efficient for scavenging •OH (9.7×10^8 M^{-1} s^{-1}), MeOH (2.5×10^8 M^{-1} s^{-1}) scavenges $SO_4^{\bullet-}$ more quickly than TBA (4–9.1×10^5 M^{-1} s^{-1}) [52,53]. In Fig. S11, after the addition of TBA and MeOH, BPA removal rates in Ag/TiO_2NTAs/PMS/VL system were reduced from 98.8% to 27.44% and 16.5%, and BPA removal rates in TiO_2NTAs/PMS/VL system were decreased from 53.1% to 22.74% and 14.5%, respectively. Combination with Fig. 3a and S3, it can be concluded that •OH and $SO_4^{\bullet-}$ were the reactive oxygen species in TiO_2NTAs/PMS/VL and Ag/TiO_2NTAs/PMS/VL systems, and •OH played a dominant role. However, in Ag/KH570/TiO_2NTAs/PMS/VL system (Fig. 5a), adding TBA and MeOH decreased BPA removal from >99.9% to 55.8% and 27.2%, respectively. MeOH did not inhibit the oxidation of BPA completely. This indicated that there were other reactive species in the Ag/KH570/TiO_2NTAs/PMS/VL system that contributed to BPA removal. In TiO_2NTAs photocatalytic

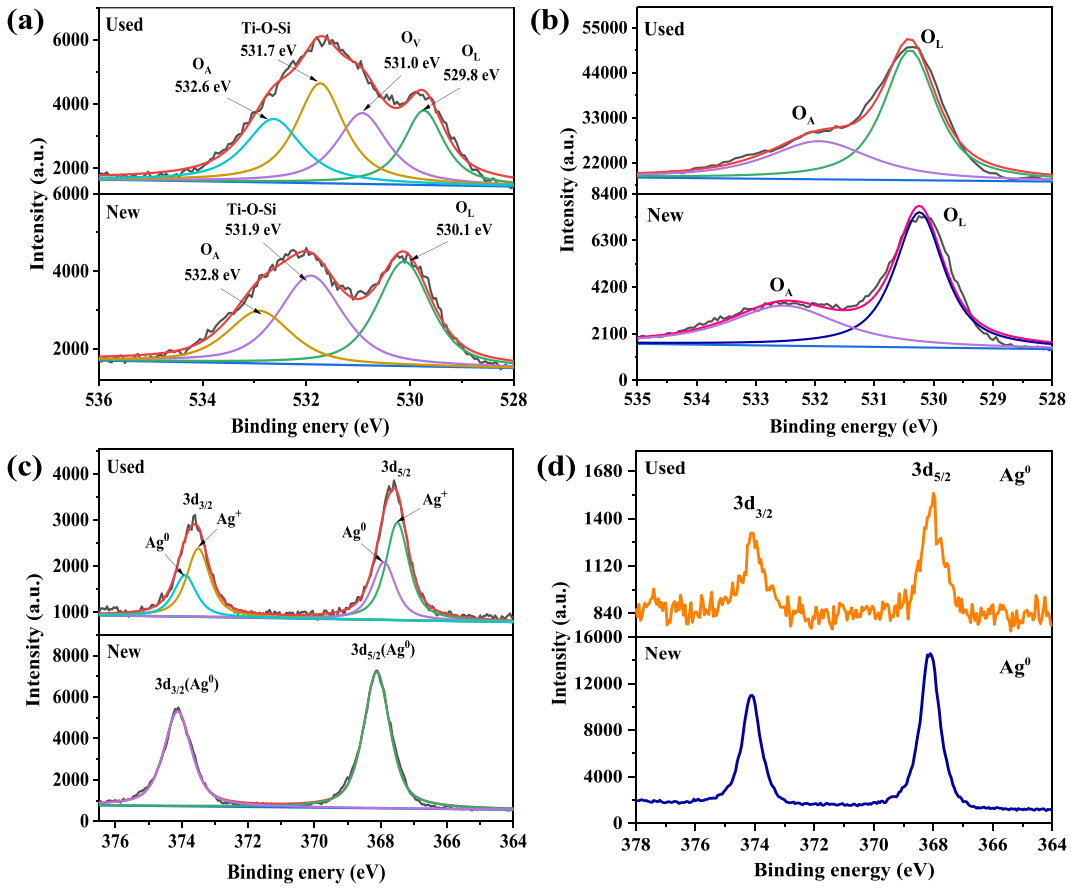

Fig. 6. High-resolution XPS spectra of the Ag 3d and O 1 s in new and used Ag/KH570/TiO_2NTAs (a, c) and Ag/TiO_2NTAs (b, d) samples.

system, holes (h^+) might also contribute to the oxidation of organics under VL irradiation (Fig. S9). EDTA-2Na as a scavenger of h^+ inhibited completely the BPA removal in Ag/KH570/TiO_2NTAs/PMS/VL system (Fig. 5a) [54], and a similar phenomenon was observed in Ag/TiO_2NTAs/PMS/VL system (Fig. S11). Nevertheless, it showed a certain inhibition (less than the inhibition of TBA) in the TiO_2NTAs/PMS/VL system (Fig. S11). The results indicated that h^+ was involved in the reaction, but it only was used for generating the •OH. Therefore, the additional BPA removal was not contributed by h^+. The complete inhibition of BPA degradation by adding EDTA-2Na might be attributed to the fact that it could chelate Ag metal [55], resulting in the failing active site. Furthermore, $^1O_2$ species, which was usually found in the PMS-based advanced oxidation process, was investigated with furfuryl alcohol (FFA) [56]. The addition of 20 mM FFA inhibited the BPA degradation from >99.9% to 11.2% (Fig. 5a), confirming the involvement of $^1O_2$ in BPA removal. It has been reported that the lifetime of $^1O_2$ in D_2O, relative to H_2O, lasted approximately ten times longer [57]. To further confirm the role of $^1O_2$, BPA degradation in D_2O was carried out, and the results showed promotion of BPA removal (Fig. 5b), thus validating the presence of $^1O_2$ from another perspective.

The EPR spectra of reactive species were examined using 5,5-dimethyl-1-pyrolin-N-oxide (DMPO) and 2,2,6,6-tetramethyl-4-piperidinol (TEMP) as spin-trapping agents (Fig. 5c). In the DMPO group, no reactive species adducts appeared in dark. Under VL irradiation, the DMPO-OH and DMPO-SO_4 adducts emerged, indicating the generation of •OH and $SO_4^{\bullet-}$, respectively. Additionally, the TEMP-$^1O_2$ adduct with a typical 1:1:1 triplet signal appeared in Fig. 5d, confirming the existence of $^1O_2$. PMS self-decomposition can slowly generate $^1O_2$ via the reaction shown in Eq. (1) [58].

$$HSO_5^- + SO_5^{2-} \rightarrow SO_4^{2-} + HSO_4^- + {}^1O_2 \quad (1)$$

Nevertheless, this process could be overlooked at pH 4.0 because of the negligible SO_5^{2-} considering the dissociation constants of PMS (pK_{a1} = 0.4 and pK_{a2} = 9.4). Previous study has reported that $O_2^{\bullet-}$ is the precursor of $^1O_2$ and has limited reactivity with BPA [59,60], so the generation of $^1O_2$ might derive from $O_2^{\bullet-}$. The $O_2^{\bullet-}$ was usually generated from a one-electron reduction of dissolved oxygen in a photocatalytic system. However, after aerating N_2 into the system (Fig. S12), BPA degradation was not inhibited, therefore ruling out the production of $^1O_2$ derived from O_2. Moreover, it is well-known that PMS reacting with Ov could form $^1O_2$. Given the absence of Ov in new Ag/KH570/TiO_2NTAs samples (Fig. 1e), it was speculated that Ov might be formed during the reaction process.

The high-resolution XPS spectra of the Ag/KH570/TiO_2NTAs after four uses (Fig. 6a) showed the characteristic peak of Ov (531.0 eV), manifesting that Ov generated during the photocatalytic activation of PMS [61,62]. No Ov formed in Ag/TiO_2NTAs/VL/PMS system (Fig. 6b). Thus, it could be concluded that the formation of Ov was closely related to KH570. In addition, the Ag chemical states of the used Ag/KH570/TiO_2NTAs were studied (Fig. 6c). Except for Ag^0 peaks, Ag^+ peaks at 367.5 eV and 373.5 eV were observed [63]. In the Ag/KH570/TiO_2NTAs/VL/PMS system, PMS could oxidize Ag^0 to Ag^+, some of which was then reduced into Ag^0 by photo-induced electrons, just like the process of Ag^+ photo-deposition on KH570/TiO_2NTAs. Due to the bridge effect of KH570, the above process could continuously occur. It was worth noting that no Ag-O bond (528.5 eV) formed in the high-resolution XPS spectrum of O 1 s (Fig. 6b) [64], thus excluding the presence of Ag_2O. Recently, during the preparation process of Ag-doped ZnO by an electrochemical deposition method, Ov would be generated by replacing Zn^{2+} sites with Ag^+ due to the difference in valence state between Ag^+ and Zn^{2+} ions [61]. Inspired by this, the continuous photo-deposition during the reaction might lead to the replacement of Ti^{4+} with Ag^+.

Table 1
Estimation of the relative contribution of reactive species on BPA degradation in Ag/KH570/TiO_2NTAs/PMS/VL process.

Process	Reactive species	Degradation rate constants of BPA (min^{-1})	Contribution (%)
Ag/KH570/TiO_2NTAs/PMS/VL	•OH + $SO_4^{\bullet-}$ + $^1O_2$ + PMS + adsorption + photolysis	0.1	100
Ag/KH570/TiO_2NTAs/PMS/VL + TBA	$SO_4^{\bullet-}$ + $^1O_2$ + PMS + adsorption + photolysis	0.0133	
Ag/KH570/TiO_2NTAs/PMS/VL + MeOH	$^1O_2$ + PMS + adsorption + photolysis	0.0051	
Ag/KH570/TiO_2NTAs/PMS/VL + FFA	PMS + adsorption + photolysis	0.0019	
	•OH		86.7
	$SO_4^{\bullet-}$		8.2
	$^1O_2$		3.2
	PMS oxidation + adsorption + photolysis		1.9

The difference in valence state between Ag^+ and Ti^{4+} ions would readily induce the generation of Ov. However, without KH570, Ag^+ and Ov could not be formed (Fig. 6).

Based on the above analyses, the enhanced catalytic degradation mechanism in Ag/KH570/TiO_2NTAs/PMS/VL system was proposed. The TiO_2NTAs could respond to VL to form e^- and h^+, and the latter reacted with OH–/H_2O to generate •OH (Eqs. (2)–(3)). The bridge function of KH570 was capable of well dispersing and solidly anchoring the Ag^0 nanoparticles on the surface of TiO_2NTAs. It dramatically enhanced the VL-induced SPR effect and the generation of photo-generated electrons (Eq. (4)). The more photo-generated electrons enabled activation of the PMS to produce more $SO_4^{\bullet-}$ and •OH (Eqs. (5)–(7)). Besides, the Ag^0 transformed to Ag^+ in the photocatalytic activation of PMS (Eq. (8)). A part of generated Ag^+ could dope into TiO_2 by replacing the Ti^{4+} sites, inducing the generation of Ov (Eq. (10)). The PMS was then trapped by Ov and transformed into $^1O_2$ (Eq. (11)) [65]. Meanwhile, the residual Ag^+ was reduced by photo-generated electrons to Ag^0 again (Eq. (9)). Because of the anchoring by KH570, the generated Ag^+ leaked into the solution scarcely and could repeat the above catalytic cycle stably (Eqs. (4)–(11)), which resulted in a highly efficient catalytic performance (Eq. (12)). The contribution proportions of reactive species were calculated based on the degradation kinetics (Fig. S13). As shown in Table 1, •OH and $SO_4^{\bullet-}$ were the main reactive species, contributing 86.7%, and 8.2% for BPA removal, respectively. However, the proportion of $^1O_2$ accounted for only 3.2%. The optimization and generation mechanism of $^1O_2$/Ov required further investigation.

$$Ag/KH570/TiO_2NTAs + h\nu \rightarrow e^- + h^+ \quad (2)$$

$$H_2O/–OH + h^+ \rightarrow \bullet OH + H^+ \quad (3)$$

$$Ag^0(\text{surface plasmon resonance}) \rightarrow Ag^0(e^-) \quad (4)$$

$$HSO_5^- + e^- \rightarrow \bullet OH + SO_4^{2-} \quad (5)$$

$$HSO_5^- + e^- \rightarrow SO_4^{\bullet-} + OH^- \quad (6)$$

$$SO_4^{\bullet-} + OH^- \rightarrow SO_4^{2-} + \bullet OH \quad (7)$$

$$Ag^0 + HSO_5^- \rightarrow Ag^+ + SO_4^{\bullet-}/SO_4^{2-} + OH^-/\bullet OH \quad (8)$$

$$Ag^+ + e^- \rightarrow Ag^0 \quad (9)$$

$$Ag^+ + TiO_2 \rightarrow Ag^+\text{-}TiO_2(Ov) \quad (10)$$

$$Ov + HSO_5^- \rightarrow {}^1O_2 + HSO_4^- \quad (11)$$

$$\bullet OH/SO_4^{\bullet-}/{}^1O_2 + BPA \rightarrow \text{degradation products} + CO_2 + H_2O \quad (12)$$

3.4. Effect of reaction parameters

Fig. 7a shows the effect of initial pH on the degradation performance of the Ag/KH570/TiO_2NTAs/PMS/VL system. The system displayed excellent performance in the pH range of 4.0–11.0. There was no significant difference in BPA degradation from pH 4.0 to 7.0. At pH=11.0, BPA could be quickly removed within 10 min. It should be pointed out that alkali was reported to be able to activate PMS, while the basic condition (pH 11) without an Ag/KH570/TiO_2NTAs only provided 14.1% of BPA removal in 60 min (Fig. S14). The increase in BPA removal efficiency by the catalyst at pH = 11.0 was not entirely due to alkali activation. Since a hydroxide ion with bare extra electrons is easier to donate an electron to PMS without activation of the H-O bond compared with water molecules to form hydroxyl radicals, the higher pH was favorable for PMS activation on an Ag/KH570/TiO_2NTAs [66]. The BPA degradation performance lowered from >99.9% to 80.7% at pH 3.0. The strong acid circumstance might cause the corrosion/leaching of the

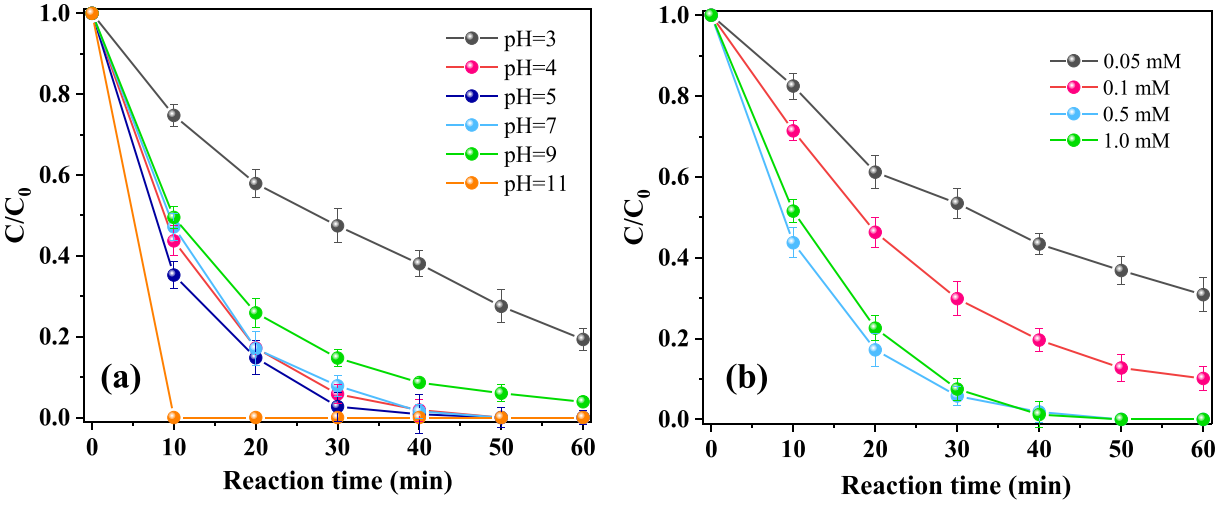

Fig. 7. Effect of initial pH value (a) and PMS concentration (b) on BPA degradation in Ag/KH570/TiO_2NTAs/PMS/VL system. Experimental conditions: $[BPA]_0$ = 10 mg/L, T = 25℃.

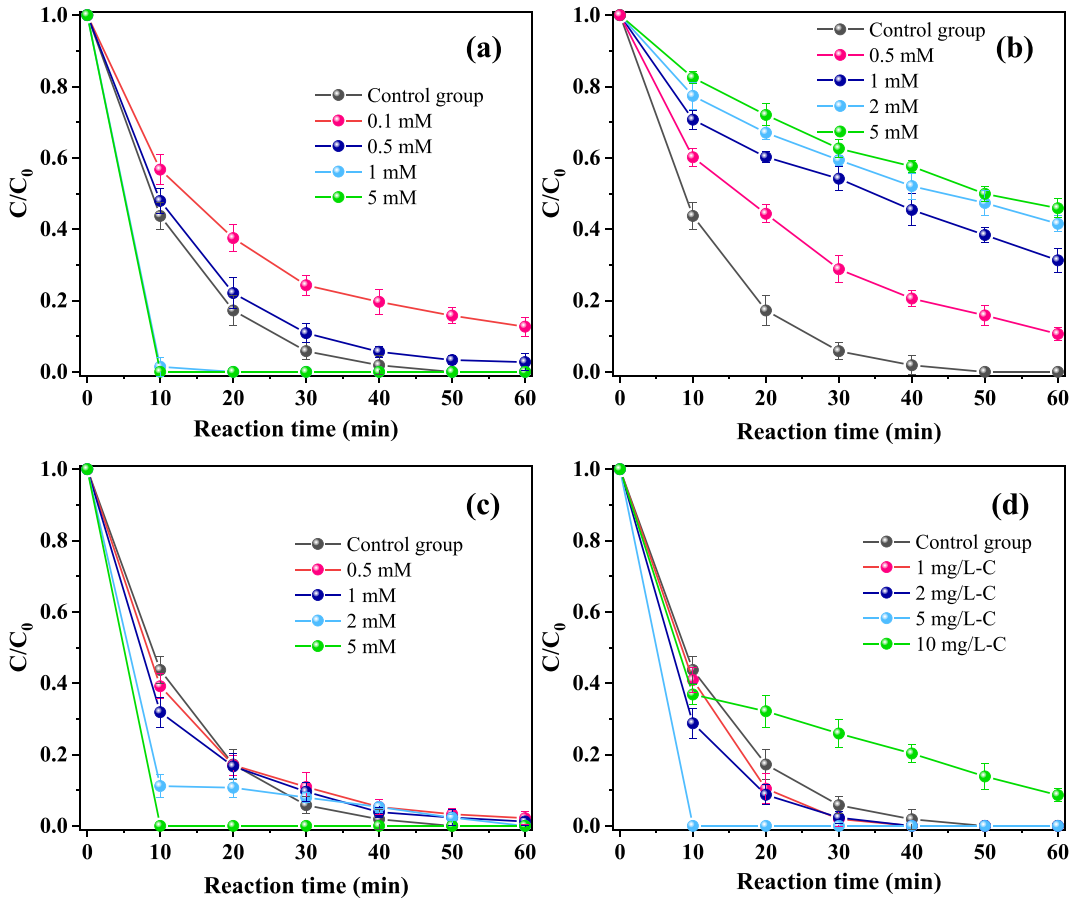

Fig. 8. Effects of (a) Cl^-, (b) NO_3^-, (c) HCO_3^-, and (d) Humic acid contents on BPA degradation. Experimental conditions: Ag/KH570/TiO_2NTAs/PMS/VL system, $[PMS]_0 = 0.5$ mM, $[BPA]_0 = 10$ mg/L, T = 25°C.

loaded Ag^0 and KH570. Overall, Ag/KH570/TiO_2NTAs were applied over a wide pH range.

Improvement of PMS concentration from 0.05 to 0.5 mM promoted the BPA degradation from 69.1% to over 99.9% (Fig. 7b). This result could be attributed to the elevated content of reactive species that were generated at higher PMS concentrations. Further improving PMS concentration to 1 mM did not lift BPA removal. Instead, it showed a slight inhibitory effect due to the self-quenching effect between PMS and reactive species. Moreover, the Ag/KH570/TiO_2NTAs/PMS/VL system was highly effective in removing low concentrations of BPA, achieving over 99.9% removal for 1 mg/L of BPA within 30 min (Fig. S15). This indicated that this system was suitable for treating organic micropollutants in water.

3.5. Effect of inorganic anions and NOM

Inorganic anions and NOM exist ubiquitously in various water bodies, and their presence can adversely affect the radical-based degradation of organics. Fig. 8 shows the catalytic performance of Ag/KH570/TiO_2NTAs/PMS/VL system in the presence of common anions and NOM. The Cl^- had dual effects on BPA degradation (Fig. 8a). Low concentration of Cl^- inhibited BPA removal, while high concentration of Cl^- exhibited a promotion effect. A similar phenomenon was also found by Hu et al [67]. The Cl^- could rapidly react with $SO_4^{\bullet-}$ and •OH to form reactive chlorine species including Cl•, $\bullet Cl_2^-$, $ClOH^{\bullet-}$, and Cl_2/HOCl [67]. Some of them (such as $\bullet Cl_2^-$) had relatively low rate constants for BPA [68]. The high concentration of Cl^- would react with PMS to produce more reactive chlorine species (HOCl and Cl_2) via the Eqs. (13)–(15) [69], which offset the radical consumption. In addition, the formed HOCl might react with photo-generated electrons to form more HO• or Cl• (Eq. (16)), resulting in an enhanced BPA removal [70].

$$HSO_5^- + Cl^- \rightarrow SO_4^{2-} + HClO \quad (13)$$

$$HSO_5^- + 2Cl^- + 2H^+ \rightarrow SO_4^{2-} + H_2O + Cl_2 \quad (14)$$

$$Cl_2 + H_2O \rightarrow HCl + HClO \quad (15)$$

$$HClO + e^- \rightarrow HO\bullet/OH^- + Cl^-/Cl\bullet \quad (16)$$

An inhibitory effect was observed when NO_3^- was added (Fig. 8a). Due to the very low reaction rates between NO_3^- and oxidants, the inhibition caused by its quenching oxidants was ruled out. The VL with low energy was unlikely to excite NO_3^- to produce NO_2^- which can scavenge radicals, so the inhibition did not come from the photolysis of nitrate [71]. The inhibition might be ascribed to the fact that NO_3^- competed with PMS for the photo-generated electrons to reduce the generation of radicals, and its reduction products (NO_2^- and NH_4^+) also consumed the reactive species [72].

The HCO_3^- is also a quencher for $SO_4^{\bullet-}$ and •OH, and they react to form carbonate radicals ($CO_3^{\bullet-}$) with low reactivity, leading to the inhibition of BPA removal in the radical-based system [73]. It was interesting that in our system, low concentration of HCO_3^- only marginally inhibited BPA degradation (around 3%), while high concentration of HCO_3^- promoted its removal significantly (Fig. 8c). Adding HCO_3^- would affect the solution pH and then promote PMS activation. When 5 mM HCO_3^- was added, the solution pH elevated from 4.0 to 9.6. At this pH, BPA degradation efficiency without HCO_3^- was 95.8% at 60 min (Fig. S16), which was lower than that of the group of 5 mM HCO_3^- (99.9% within 10 min), suggesting that the improving pH was not responsible for the enhanced BPA removal. The increase of HCO_3^- content might improve the steady-state concentration of $CO_3^{\bullet-}$ or induce the

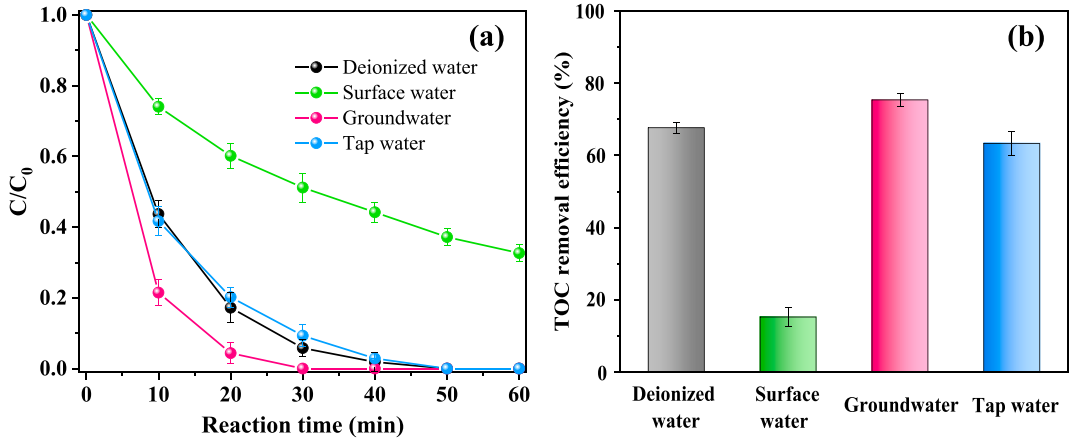

Fig. 9. Degradation of BPA (a) and removal of TOC (b) by Ag/KH570/TiO_2NTAs in actual water samples. Experimental conditions: $[PMS]_0 = 0.5$ mM, $[BPA]_0 = 10$ mg/L, T = 25℃, TOC removal time = 120 min.

generation of $^1O_2$ via the Eqs. (17)–(18), which not only compensated for its smaller reactivity and consumption of radicals but also degraded more BPA [74,75].

$$CO_{3ads}^{2-} + HSO_5^- \rightarrow SO_5^{\bullet -} + HCO_3^- + e^- \quad (17)$$

$$SO_5^{\bullet -} + SO_5^{\bullet -} \rightarrow S_2O_8^{2-} + {}^1O_2 \quad (18)$$

Increasing humic acid concentration from 0 to 5 mg/L accelerated BPA removal dramatically. Generally, humic acid acts as a scavenger for radicals. However, our previous study has suggested that under VL irradiation, humic acid containing aromatic constituents/phenolic groups could be excited to generate e_{aq}^- and excited state humic acid, which could activate PMS to generate the reactive species [76]. This mechanism could also apply to this study, which explained the accelerated removal of BPA. As the concentration of humic acid improved to 10 mg/L, the BPA degradation was suppressed. This was because the higher humic acid content competed with BPA for radicals and increased the turbidity of the solution, impeding the transmission of VL. Nonetheless, the BPA removal efficiency remained above 90%, implying that the system is high resistance to the NOM.

3.6. Application in actual water sample

The application potential of Ag/KH570/TiO_2NTAs/PMS/VL system in actual water sample was investigated. As shown in Fig. 9, the degradation efficiency of BPA in deionized water was comparable to that in tap water. The BPA removal in groundwater was enhanced, while it was inhibited in surface water. Furthermore, the results of mineralization were similar to those of BPA removal, with the mineralization efficiencies of 75%, 68%, 63%, and 15% in groundwater, deionized water, tap water, and surface water, respectively. In general, the photocatalytic performance in actual water sample was hindered, especially in water with bicarbonate or NOM that could scavenge radicals. It was observed that the different water matrices exerted opposing effects on BPA removal, including promotion and inhibition. The results suggested that the promotion effect offset the inhibition influence in tap water, and the high concentration of Cl^- and HCO_3^- in groundwater contributed to the improvement of BPA removal (Table S2). The suppression of BPA removal in surface water could be attributed to factors such as TOC, NO_3^-, and low concentration of Cl^-. In addition, PO_4^{3-} could also scavenge $SO_4^{\bullet -}$ and •OH to produce H_2PO_4• with low reactivity, resulting in an inferior performance.

4. Conclusions

In summary, we successfully synthesized a stable Ag-modified TiO_2NTAs with KH570 as the binder for VL photocatalytic activation of PMS. The Ag/KH570/TiO_2NTAs/PMS/VL system exhibited excellent removal performance for BPA with minimal Ag leaching even after 30 cycles, which was ascribed to the bridge function of KH570. On the one hand, the KH570 could disperse well Ag on the surface of TiO_2NTAs, which improved VL absorption and photo-electrochemical performances. On the other hand, KH570 anchored firmly Ag on the surface of TiO_2NTAs, which ensured continuous generation of photo-generated electrons and Ag^0, thus leading to efficient PMS activation. Mechanism analysis showed that •OH and $SO_4^{\bullet -}$ oxidations played the dominant role in the removal of BPA. The Ag/KH570/TiO_2NTAs/PMS/VL system was suitable for a wide pH range (4–11) and low concentrations of BPA. The proper presence of Cl^-, HCO_3^-, and humic acid generated more reactive species for enhanced removal of BPA, which were the reason that BPA was effectively removed in actual water samples (groundwater and tap water). In the future, we would develop a decentralized drinking water treatment device using Ag/KH570/TiO_2NTAs catalyst under actual solar irradiation.

CRediT authorship contribution statement

Jialin Jia: Conceptualization, Investigation, Data curation, Formal analysis, Validation, Writing – original draft. **Stefanos Giannakis:** Writing - review & editing. **Dong Li:** Investigation, Formal analysis, Methodology, Writing - original draft, Writing - review & editing. **Tao Lin:** Project administration. **Jiayu Tian:** Supervision. **Dongmei Liu:** Funding acquisition, Supervision. **Jun Ma:** Resources.

Declaration of Competing Interest

The authors declare that they have no known competing financial interests or personal relationships that could have appeared to influence the work reported in this paper.

Data availability

No data was used for the research described in the article.

Acknowledgments

This work was supported by the funds of the State Key Laboratory of Urban Water Resource and Environment (HIT, 2022TS03), China Scholarship Council (No. 202006120369), National Key P&D Program of China (2022YFC3203702), the Science and Technology Development Plans of Ministry of Housing and Urban-Rural Development (2021-K-131), the Six Talent Peaks Project in Jiangsu Province (JNHB-004), and

Stefanos Giannakis acknowledges the Spanish Ministry of Science, Innovation and Universities (MICIU) for the Ramón y Cajal Fellowship (RYC2018-024033-I).

Appendix A. Supplementary data

Supplementary data to this article can be found online at https://doi.org/10.1016/j.seppur.2023.124029.

References

[1] M. Kohantorabi, G. Moussavi, S. Giannakis, A review of the innovations in metal- and carbon-based catalysts explored for heterogeneous peroxymonosulfate (PMS) activation, with focus on radical vs. non-radical degradation pathways of organic contaminants, Chem. Eng. J. 411 (2021), 127957.
[2] D. Li, H. He, J. Jia, W. Shi, F. Yin, J. Yu, M. Chen, J. Ma, Mitigation of ultrafiltration membrane fouling by a simulated sunlight-peroxymonosulfate system with the assistance of irradiated NOM, Water Res. 229 (2023), 119452.
[3] Y. Yang, G. Banerjee, G.W. Brudvig, J.-H. Kim, J.J. Pignatello, Oxidation of organic compounds in water by unactivated peroxymonosulfate, Environ. Sci. Tech. 52 (2018) 5911–5919.
[4] J. Wang, S. Wang, Activation of persulfate (PS) and peroxymonosulfate (PMS) and application for the degradation of emerging contaminants, Chem. Eng. J. 334 (2018) 1502–1517.
[5] F. Ghanbari, M. Moradi, Application of peroxymonosulfate and its activation methods for degradation of environmental organic pollutants: review, Chem. Eng. J. 310 (2017) 41–62.
[6] A.B. Alayande, S. Hong, Ultraviolet light-activated peroxymonosulfate (UV/PMS) system for humic acid mineralization: effects of ionic matrix and feasible application in seawater reverse osmosis desalination, Environ. Pollut. 307 (2022), 119513.
[7] Y. Lee, S. Lee, M. Cui, Y. Ren, B. Park, J. Ma, Z. Han, J. Khim, Activation of peroxodisulfate and peroxymonosulfate by ultrasound with different frequencies: impact on ibuprofen removal efficient, cost estimation and energy analysis, Chem. Eng. J. 413 (2021), 127487.
[8] J. Li, J. Zou, S. Zhang, H. Cai, Y. Huang, J. Lin, Q. Li, B. Yuan, J. Ma, Sodium tetraborate simultaneously enhances the degradation of acetaminophen and reduces the formation potential of chlorinated by-products with heat-activated peroxymonosulfate oxidation, Water Res. 224 (2022), 119095.
[9] Y. Mao, H. Dong, S. Liu, L. Zhang, Z. Qiang, Accelerated oxidation of iopamidol by ozone/peroxymonosulfate (O3/PMS) process: kinetics, mechanism, and simultaneous reduction of iodinated disinfection by-product formation potential, Water Res. 173 (2020), 115615.
[10] Z. Bai, S. Gao, H. Yu, X. Liu, J. Tian, Layered metal oxides loaded ceramic membrane activating peroxymonosulfate for mitigation of NOM membrane fouling, Water Res. 222 (2022), 118928.
[11] X. Zheng, X. Niu, D. Zhang, M. Lv, X. Ye, J. Ma, Z. Lin, M. Fu, Metal-based catalysts for persulfate and peroxymonosulfate activation in heterogeneous ways: a review, Chem. Eng. J. 429 (2022) 132323.
[12] Y. Fang, H. Wang, X. Wang, Y. Zhou, L. Wu, W.D. Wu, Z. Wu, Constructing thin BiOCl nanoplates for highly efficient photocatalytic peroxymonosulfate activation: in-depth understanding of the activation process, Sep. Purif. Technol. 307 (2023) 122771.
[13] Q. Sun, Y. Zhao, J. Zhang, J. Sheng, Efficient degradation of antibiotics over Co(II)-doped Bi2MoO6 nanohybrid via the synergy of peroxymonosulfate activation and photocatalytic reaction under visible irradiation, Chemosphere 302 (2022), 134807.
[14] C. Yao, Z. Wang, Z. Xu, B. Jiang, Y. Yang, S. Wang, 2D/2D α-Fe2O3/single-layer MXene Schottky photocatalysis-PMS activation bidirectionally enhanced coupling system for environmental remediation, J. Alloy. Compd. 941 (2023), 168920.
[15] J. Jia, D. Liu, Q. Wang, H. Li, J. Ni, F. Cui, J. Tian, Comparative study on bisphenols oxidation via TiO2 photocatalytic activation of peroxymonosulfate: effectiveness, mechanism and pathways, J. Hazard. Mater. 424 (2022) 127434.
[16] J. Jia, D. Liu, S. Wang, H. Li, J. Ni, X. Li, J. Tian, Q. Wang, Visible-light-induced activation of peroxymonosulfate by TiO2 nano-tubes arrays for enhanced degradation of bisphenol A, Sep. Purif. Technol. 253 (2020), 117510.
[17] T. Wang, J. Zhou, W. Wang, Y. Zhu, J. Niu, Ag-single atoms modified S1.66-N1.91/TiO2-x for photocatalytic activation of peroxymonosulfate for bisphenol A degradation, Chin. Chem. Lett. 33 (2022) 2121–2124.
[18] O. Mertah, A. Gómez-Avilés, A. Kherbeche, C. Belver, J. Bedia, Peroxymonosulfate enhanced photodegradation of sulfamethoxazole with TiO2@CuCo2O4 catalysts under simulated solar light, J. Environ. Chem. Eng. 10 (2022), 108438.
[19] G.A. Ashraf, R.T. Rasool, R.U. Rasool, M.F. Saleem, J. Ali, D. Ghernaout, M. Hassan, A.M. Aljuwayid, M.A. Habila, H. Guo, Photocatalytic stimulation of peroxymonosulfate by novel MoO3@ZrO2 with Z-scheme heterojunction for diclofenac sodium degradation, J. Water Process Eng. 51 (2023), 103435.
[20] Z. Li, W. Ai, Y. Zhang, J. Zhang, W. Liu, D. Zhong, Y. Cai, E. Johansson, G. Boschloo, W. Jin, L. Yang, Magnetic carbon nanotube modified S-scheme TiO2-x/g-C3N4/CNFe heterojunction coupled with peroxymonosulfate for effective visible-light-driven photodegradation via enhanced interfacial charge separation, Sep. Purif. Technol. 308 (2023), 122897.
[21] X. Zhang, J. Duan, Y. Tan, Y. Deng, C. Li, Z. Sun, Insight into peroxymonosulfate assisted photocatalysis over Fe2O3 modified TiO2/diatomite composite for highly efficient removal of ciprofloxacin, Sep. Purif. Technol. 293 (2022), 121123.
[22] G. Alnaggar, A. Hezam, M.A. Bajiri, Q.A. Drmosh, S. Ananda, Sulfate radicals induced from peroxymonosulfate on electrochemically synthesized TiO2–MoO3 heterostructure with Ti–O–Mo bond charge transfer pathway for potential organic pollutant removal under solar light irradiation, Chemosphere 303 (2022), 134562.
[23] M. Wang, T. Li, Q. Hou, Y. Hao, Z. Wang, Facile one-step preparation of Co and Ce doped TiO2 in visible light PMS activation for PAHs degradation, Chemosphere 308 (2022), 136360.
[24] M. Kohantorabi, G. Moussavi, S. Mohammadi, P. Oulego, S. Giannakis, Photocatalytic activation of peroxymonosulfate (PMS) by novel mesoporous Ag/ZnO@NiFe2O4 nanorods, inducing radical-mediated acetaminophen degradation under UVA irradiation, Chemosphere 277 (2021), 130271.
[25] M. Sayed, B. Ren, A.M. Ali, A. Al-Anazi, M.N. Nadagouda, A.A. Ismail, D. D. Dionysiou, Solar light induced photocatalytic activation of peroxymonosulfate by ultra-thin Ti3+ self-doped Fe2O3/TiO2 nanoflakes for the degradation of naphthalene, Appl. Catal. B 315 (2022), 121532.
[26] D. Li, J. Jia, T. Zheng, X. Cheng, X. Yu, Construction and characterization of visible light active Pd nano-crystallite decorated and C-N-S-co-doped TiO2 nanosheet array photoelectrode for enhanced photocatalytic degradation of acetylsalicylic acid, Appl. Catal. B 188 (2016) 259–271.
[27] A. Cabrera-Reina, A.B. Martínez-Piernas, Y. Bertakis, N.P. Xekoukoulotakis, A. Agüera, J.A. Sánchez Pérez, TiO2 photocatalysis under natural solar radiation for the degradation of the carbapenem antibiotics imipenem and meropenem in aqueous solutions at pilot plant scale, Water Res. 166 (2019), 115037.
[28] M.J. Nalbandian, K.E. Greenstein, D. Shuai, M. Zhang, Y.-H. Choa, G.F. Parkin, N. V. Myung, D.M. Cwiertny, Tailored synthesis of photoactive TiO2 nanofibers and Au/TiO2 nanofiber composites: structure and reactivity optimization for water treatment applications, Environ. Sci. Tech. 49 (2015) 1654–1663.
[29] H.Y. Yoo, M.S. Kim, H. Shin, J. Lim, Peroxymonosulfate activation by black TiO2 nanotube arrays under solar light: switching the activation mechanism and enhancing catalytic activity and stability, J. Hazard. Mater. 433 (2022), 128796.
[30] X. Cheng, Q. Cheng, B. Li, X. Deng, J. Li, P. Wang, B. Zhang, H. Liu, X. Wang, One-step construction of N/Ti3+ codoped TiO2 nanotubes photoelectrode with high photoelectrochemical and photoelectrocatalytic performance, Electrochim. Acta 186 (2015) 442–448.
[31] A. Tamilselvan, D. Durgalakshmi, R. Ajay Rakkesh, S. Balakumar, Enhanced photocatalytic activity of TiO2 nanotubes arrays decorated with Ag and Pt nanoparticles, Mater. Today:. Proc. 64 (2022) 1822–1831.
[32] Y. Cheng, J. Gao, Q. Shi, Z. Li, W. Huang, In situ electrochemical reduced Au loaded black TiO2 nanotubes for visible light photocatalysis, J. Alloy. Compd. 901 (2022), 163562.
[33] D. Li, X. Zhang, W. Zhang, Designing a new reaction system by stacking use of Ti mesh supported Ag/N-TiO2 nano-sheets for enhanced photocatalytic degradation of bisphenol A, Chem. Eng. J. 405 (2021), 126867.
[34] S. Zhang, F. Peng, H. Wang, H. Yu, S. Zhang, J. Yang, H. Zhao, Electrodeposition preparation of Ag loaded N-doped TiO2 nanotube arrays with enhanced visible light photocatalytic performance, Catal. Commun. 12 (2011) 689–693.
[35] Y. Hou, X. Li, Q. Zhao, G. Chen, C.L. Raston, Role of hydroxyl radicals and mechanism of *Escherichia coli* inactivation on Ag/AgBr/TiO2 nanotube array electrode under visible light irradiation, Environ. Sci. Tech. 46 (2012) 4042–4050.
[36] J. Sang, S. Aisawa, K. Miura, H. Hirahara, O. Jan, P. Jozef, M. Pavol, Adhesion of carbon steel and natural rubber by functionalized silane coupling agents, Int. J. Adhes. Adhes. 72 (2017) 70–74.
[37] W. Zheng, C. Tang, J. Xie, Y. Gui, Micro-scale effects of nano-SiO2 modification with silane coupling agents on the cellulose/nano-SiO2 interface, Nanotechnology 30 (2019), 445701.
[38] S. Fu, X. Zhao, Z. Zhou, M. Li, L. Zhu, Effective removal of odor substances using intimately coupled photocatalysis and biodegradation system prepared with the silane coupling agent (SCA)-enhanced TiO2 coating method, Water Res. 188 (2021), 116569.
[39] X.-H. Pan, L.-X. Fu, H. Wang, Y. Xue, J.-H. Zu, Synthesis of novel sulfydryl-functionalized chelating adsorbent and its application for selective adsorption of Ag(I) under high acid, Sep. Purif. Technol. 271 (2021), 118778.
[40] L. Xu, Y. Liu, J. Wang, Y. Tang, Z. Zhang, Selective adsorption of Pb2+ and Cu2+ on amino-modified attapulgite: kinetic, thermal dynamic and DFT studies, J. Hazard. Mater. 404 (2021) 124140.
[41] S. Hao, A. Verlotta, P. Aprea, F. Pepe, D. Caputo, W. Zhu, Optimal synthesis of amino-functionalized mesoporous silicas for the adsorption of heavy metal ions, Microporous Mesoporous Mater. 236 (2016) 250–259.
[42] J. Burgess, P.J. Steel, Is the silver–alkene interaction a useful new supramolecular synthon? Coord. Chem. Rev. 255 (2011) 2094–2103.
[43] Y.-C. Liu, X. Liu, G.-H. Zhang, W. Liu, J.-Q. Wang, X. Wang, C.-L. Chen, Y. Wang, Z. Xiang, Performance and mechanism of a novel S-scheme heterojunction sonocatalyst CuS/BaWO4 for degradation of bisphenol A by ultrasonic activation, Environ. Res. 216 (2023), 114720.
[44] J. Jia, D. Li, J. Wan, X. Yu, Characterization and mechanism analysis of graphite/C-doped TiO2 composite for enhanced photocatalytic performance, J. Ind. Eng. Chem. 33 (2016) 162–169.
[45] J. Chen, H. Che, K. Huang, C. Liu, W. Shi, Fabrication of a ternary plasmonic photocatalyst CQDs/Ag/Ag2O to harness charge flow for photocatalytic elimination of pollutants, Appl. Catal. B 192 (2016) 134–144.
[46] P. Zhang, X. Li, X. Wu, T. Zhao, L. Wen, Influence of In3+-doping and Ag0-depositing on the visible-light-induced photocatalytic activity of TiO2, J. Alloy. Compd. 673 (2016) 405–410.

[47] X. Guo, D. Li, J. Wan, X. Yu, Preparation and electrochemical property of TiO2/Nano-graphite composite anode for electro-catalytic degradation of ceftriaxone sodium, Electrochim. Acta 180 (2015) 957–964.
[48] G. Lu, S.L. Bernasek, J. Schwartz, Oxidation of a polycrystalline titanium surface by oxygen and water, Surf. Sci. 458 (2000) 80–90.
[49] S. Rasalingam, H.S. Kibombo, C.-M. Wu, S. Budhi, R. Peng, J. Baltrusaitis, R. T. Koodali, Influence of Ti–O–Si hetero-linkages in the photocatalytic degradation of Rhodamine B, Catal. Commun. 31 (2013) 66–70.
[50] L. Zhang, L. Rao, P. Wang, Z. Shi, P. Wang, Superhydrophobic self-floating TiO2-silicone composite aerogels and their air–liquid-solid triphase photocatalytic system, Appl. Surf. Sci. 536 (2021), 147726.
[51] A. Wang, Q. Zhu, Z. Xing, Multifunctional quaternized chitosan@surface plasmon resonance Ag/N-TiO2 core-shell microsphere for synergistic adsorption-photothermal catalysis degradation of low-temperature wastewater and bacteriostasis under visible light, Chem. Eng. J. 393 (2020), 124781.
[52] H. Song, L. Yan, J. Ma, J. Jiang, G. Cai, W. Zhang, Z. Zhang, J. Zhang, T. Yang, Nonradical oxidation from electrochemical activation of peroxydisulfate at Ti/Pt anode: efficiency, mechanism and influencing factors, Water Res. 116 (2017) 182–193.
[53] G.V. Buxton, C.L. Greenstock, W.P. Helman, A.B. Ross, Critical Review of rate constants for reactions of hydrated electrons, hydrogen atoms and hydroxyl radicals (·OH/·O− in Aqueous Solution, J. Phys. Chem. Ref. Data 17 (1988) 513–886.
[54] Y. Chi, W. Wang, Q. Zhang, H. Yu, M. Liu, S. Ni, B. Gao, S. Xu, Evaluation of practical application potential of a photocatalyst: ultimate apparent photocatalytic activity, Chemosphere 285 (2021), 131323.
[55] E.F.C. Chaúque, J.C. Ngila, S.C. Ray, L. Ndlwana, Degradation of methyl orange on Fe/Ag nanoparticles immobilized on polyacrylonitrile nanofibers using EDTA chelating agents, J. Environ. Manage. 236 (2019) 481–489.
[56] Y. Zhou, J. Jiang, Y. Gao, J. Ma, S.-Y. Pang, J. Li, X.-T. Lu, L.-P. Yuan, Activation of peroxymonosulfate by benzoquinone: a novel nonradical oxidation process, Environ. Sci. Tech. 49 (2015) 12941–12950.
[57] E.-T. Yun, J.H. Lee, J. Kim, H.-D. Park, J. Lee, Identifying the nonradical mechanism in the peroxymonosulfate activation process: singlet oxygenation versus mediated electron transfer, Environ. Sci. Tech. 52 (2018) 7032–7042.
[58] H. Li, C. Shan, B. Pan, Fe(III)-doped g-C3N4 mediated peroxymonosulfate activation for selective degradation of phenolic compounds via high-valent iron-oxo species, Environ. Sci. Tech. 52 (2018) 2197–2205.
[59] R. Luo, M. Li, C. Wang, M. Zhang, M.A. Nasir Khan, X. Sun, J. Shen, W. Han, L. Wang, J. Li, Singlet oxygen-dominated non-radical oxidation process for efficient degradation of bisphenol A under high salinity condition, Water Res. 148 (2019) 416–424.
[60] L. Wu, Z. Sun, Y. Zhen, S. Zhu, C. Yang, J. Lu, Y. Tian, D. Zhong, J. Ma, Oxygen vacancy-induced nonradical degradation of organics: critical trigger of oxygen (O2) in the Fe–Co LDH/peroxymonosulfate system, Environ. Sci. Tech. 55 (2021) 15400–15411.
[61] J. Li, Y. Li, S. Li, M. Zhu, J. Zhang, Y. Li, Y. He, W. Li, Zinc interstitial and oxygen vacancy mediated high Curie-temperature ferromagnetism in Ag-doped ZnO, Ceram. Int. 46 (2020) 18639–18647.
[62] X. Dong, X. Duan, Z. Sun, X. Zhang, C. Li, S. Yang, B. Ren, S. Zheng, D.D. Dionysiou, Natural illite-based ultrafine cobalt oxide with abundant oxygen-vacancies for highly efficient Fenton-like catalysis, Appl. Catal. B 261 (2020), 118214.
[63] M.A. Thomas, W.W. Sun, J.B. Cui, Mechanism of Ag doping in ZnO nanowires by electrodeposition: experimental and theoretical insights, J. Phys. Chem. C 116 (2012) 6383–6391.
[64] Y. Cui, Q. Ma, X. Deng, Q. Meng, X. Cheng, M. Xie, X. Li, Q. Cheng, H. Liu, Fabrication of Ag-Ag2O/reduced TiO2 nanophotocatalyst and its enhanced visible light driven photocatalytic performance for degradation of diclofenac solution, Appl. Catal. B 206 (2017) 136–145.
[65] P. Gao, X. Tian, Y. Nie, C. Yang, Z. Zhou, Y. Wang, Promoted peroxymonosulfate activation into singlet oxygen over perovskite for ofloxacin degradation by controlling the oxygen defect concentration, Chem. Eng. J. 359 (2019) 828–839.
[66] X. Duan, C. Su, L. Zhou, H. Sun, A. Suvorova, T. Odedairo, Z. Zhu, Z. Shao, S. Wang, Surface controlled generation of reactive radicals from persulfate by carbocatalysis on nanodiamonds, Appl. Catal. B 194 (2016) 7–15.
[67] L. Hu, G. Zhang, M. Liu, Q. Wang, P. Wang, Enhanced degradation of Bisphenol A (BPA) by peroxymonosulfate with Co3O4-Bi2O3 catalyst activation: effects of pH, inorganic anions, and water matrix, Chem. Eng. J. 338 (2018) 300–310.
[68] Y. Lei, S. Cheng, N. Luo, X. Yang, T. An, Rate constants and mechanisms of the reactions of Cl• and Cl2•− with trace organic contaminants, Environ. Sci. Tech. 53 (2019) 11170–11182.
[69] Z. Wang, R. Yuan, Y. Guo, L. Xu, J. Liu, Effects of chloride ions on bleaching of azo dyes by Co2+/oxone regent: kinetic analysis, J. Hazard. Mater. 190 (1-3) (2011) 1083–1087.
[70] H.-C. Zhang, Y.-L. Liu, L. Wang, Z.-Y. Li, X.-H. Lu, T. Yang, J. Ma, Enhanced radical generation in an ultraviolet/chlorine system through the addition of TiO2, Environ. Sci. Tech. 55 (2021) 11612–11623.
[71] O. Mertah, K. El Hajjaji, S. El Amrani, K. Tanji, I. Goncharova, A. Kherbeche, Visible-light Cu/TiO2@Ag3PO4 heterostructure photocatalyst for selective nitrate reduction and antimicrobial activity, Opt. Mater. 129 (2022), 112549.
[72] H. Shi, C. Li, L. Wang, W. Wang, J. Bian, X. Meng, Photocatalytic reduction of nitrate pollutants by novel Z-scheme ZnSe/BiVO4 heterostructures with high N2 selectivity, Sep. Purif. Technol. 300 (2022), 121854.
[73] C. Guan, J. Jiang, S. Pang, X. Chen, R.D. Webster, T.-T. Lim, Facile synthesis of pure g-C3N4 materials for peroxymonosulfate activation to degrade bisphenol A: effects of precursors and annealing ambience on catalytic oxidation, Chem. Eng. J. 387 (2020), 123726.
[74] J. Gao, X. Duan, K. O'Shea, D.D. Dionysiou, Degradation and transformation of bisphenol A in UV/Sodium percarbonate: dual role of carbonate radical anion, Water Res. 171 (2020), 115394.
[75] X. Wang, Y. Zhou, N. Wang, J. Zhang, L. Zhu, Carbonate-induced enhancement of phenols degradation in CuS/peroxymonosulfate system: a clear correlation between this enhancement and electronic effects of phenols substituents, J. Environ. Sci. 129 (2023) 139–151.
[76] J. Jia, D. Liu, J. Tian, W. Wang, J. Ni, X. Wang, Visible-light-excited humic acid for peroxymonosulfate activation to degrade bisphenol A, Chem. Eng. J. 400 (2020), 125853.